Scattered light diagnostics of overdense plasma cavity in solid targets irradiated by an ultraintense laser pulse

A. A. Andreev,[1] A. G. Zhidkov,[2] M. Uesaka,[2] K. Kinoshita,[2] and K. Yu. Platonov[1]
[1]*Institute for Laser Physics, St. Petersburg, 12 Birzhevaya Line, 119064, Russia*
[2]*NERL, School of Engineering, University of Tokyo, 22-2 Shirane-shirakata, Tokai, Naka, Ibaraki 319-1188, Japan*
(Received 30 November 2001; revised manuscript received 14 June 2002; published 24 September 2002)

The light scattered backward from a target illuminated by ultraintense laser pulses carries important information about the nonlinear laser-plasma interaction. We analyze the usefulness of this information by plasma corona analysis with the help of an analytical model we developed, and particl-in-cell simulation. The spectrum of scattered light is shown to be shifted, to be broadened, and to be modulated, in comparison with the initial laser spectrum, and the spectral shift is an indicator of laser pulse contrast ratio.

DOI: 10.1103/PhysRevE.66.036405 PACS number(s): 52.38.−r

INTRODUCTION

Measurement of the spectrum of scattered laser radiation is an important method for the investigation of dense laser plasmas [1,2]. This method can be particularly useful for studying the plasma corona produced by the laser prepulse that inevitably precedes an intense short laser pulse [3,4]. However, to reconstruct plasma parameters from results of spectral measurements, one has, at first, to find the exact connection between these parameters and the spectrum. We have attempted to do this in our earlier papers [5,6]. In a recent paper [7], the phase of the reflected wave has been found by numerical simulation. In the present paper we study the dynamics of plasma in strong laser fields via numerical simulation and analytical modeling.

We consider slow ion plasma movements only, and their influence on the reflected wave spectrum. In such case from low ion velocities, the shift of scattered wave frequency and spectrum width are small compared to the laser frequency. The structure of nonlinear plasma density oscillations is evaluated on the basis of our developed analytical model and confirmed by simulations. The shift and width of the spectrum of the scattered radiation are obtained and attributed to the laser pulse parameters. At high laser pulse intensities, the spectrum is shown to be dominated not only by the movement of the critical density surface, which was obtained earlier [1], but also by the generation of nonlinear density oscillations in the plasma.

A. Collision particle-in-cell method

We apply a collisional particle-in-cell PIC method to simulate the interaction of a plasma layer with an intense ultrashort laser pulse. The method is based on the collisional electromagnetic PIC and is appropriate for the analysis of the dynamics of overdense plasmas created by an arbitrary polarized, obliquely incident pulse laser. The method employs the Langevin equation to account for elastic collisions and non-local-thermodynamic-equilibrium average ion model for plasma ionization including the ionization due to the laser as well as plasma field. The details of the method can be found in Ref. [11]. The 1–2/2D (where D stands for dimension) relativistic electromagnetic, multicomponent PIC code with a square-law current and charge weighting is used to calculate the interaction of an intense obliquely incident pulse laser with an overdense plasma. Collisions are computed as an effective force after calculation of the velocity and position of CP. The calculation with movable ions is carried out for plasmas with a variable initial density profile. In the present work, to exclude the effect of ionization, we fix the ion charge $Z=10$. Simulations are performed at wavelengths of 1 μm for laser intensity $I \geqslant 10^{16}$ W/cm^2. The laser intensity is kept constant during the pulse duration. The incident angle of the pulse is 0°. The time step is set to $0.03/\omega_p^0$, where ω_p^0 is the initial plasma frequency. The number of CPs is 5×10^4 per 1 μm of the plasma. The thickness of the plasma layer varies from 1 to several micrometers.

B. Analytical model

1. Basic equations of analytical model

To formulate the general dependences of the considered processes and understand the simulation results we developed the analytical model. We consider a linearly polarized laser wave that propagates in the opposite direction to the z axis and interacts with an overdense plasma layer, in hydrodynamic approximation. The law of conservation of electron transverse canonical momentum allows us to reduce the system of hydrodynamic equations of electron motion and Maxwell equations to two nonlinear differential equations for linearly polarized electromagnetic wave vector potential $A_x(z;t)$ and longitudinal electric field $E_z(z;t)$ in the plasma [6]. We average over plasma oscillation period these equations and use the approximation of quasineutrality. Then, for the amplitude of vector potential the next equation follows:

$$\left(\frac{\partial^2}{\partial\xi^2}+2i\frac{\delta_s}{\Omega_p}\frac{\partial}{\partial\tau}+\frac{1}{\Omega_p^2}\right)A=\left(\eta+\frac{\partial^2}{\partial\xi^2}\sqrt{1+A^2}\right)\frac{A}{\sqrt{1+A^2}}. \tag{1}$$

With Eq. (1), we can formulate equations of motion for the ionic component,

$$\frac{\partial\eta}{\partial\tau}+\frac{\partial}{\partial\xi}(\eta\mu)=0,$$

$$\frac{\partial \mu}{\partial \tau}+\mu\frac{\partial \mu}{\partial \xi}+\frac{\partial}{\partial \xi}\ln \eta=\delta_T^{-2}\frac{\partial\sqrt{1+A^2}}{\partial \xi}. \tag{2}$$

In Eq. (1) and (2), the following dimensionless variables are used: $\xi=(\omega_p/c)z$, $\tau=\delta_s\psi_p t$. Here $c_s=\sqrt{ZT_c/M}$, $\delta_s=c_s/c$, $eA_x(\xi,\tau)/mc^2=A(\xi,\tau)\exp(-i\tau\omega_0/\omega_p)$, ω_0-laser frequency, $E(\xi,\tau)=eE_z/mc\omega_p$; $\delta_T=v_{\mathrm{Te}}c$; v_{Te} is electron thermal velocity; $\omega_p=(4\pi Zn_{i0}e^2/m)^{1/2}$ being electron plasma frequency, $\Omega_p=\omega_p/\omega_0$, $\eta(\xi,\tau)=n_i(\xi,\tau)/n_{i0}$ being dimensionless profile of ion density in the plasma, n_{i0} is maximal ion density inside overdense plasma, $\mu(\xi,\tau)=v_i/c_s$ is dimensionless ion velocity. In the used approximation of quasineutrality the field E_z is connected with A_x by the equation [6],

$$E=\frac{\partial}{\partial \xi}\sqrt{1+A^2}+\delta_T^2\frac{\partial}{\partial \xi}\ln \eta.$$

2. Model plasma parameters

If the laser pulse t_L is shorter than l_s/c_s (where $l_s=c/\omega_p$ is length of the skin layer), the pressure of the laser field is equivalent to the instantaneous shock on the plasma. In this case $A(\xi,\tau)\sim A(\xi)\delta(\tau/\tau_L)$, and then $v|_{\tau=0}\approx\tau_L/\delta_T^2\sqrt{1+A^2}/\ell_s$, where $\tau_L=\delta_s\omega_p t_L$. For a homogeneous system (2), the solution of a problem involving such instantaneous shock is explained by an example in Ref. [8].

Any analytical solution of Eqs. (1) and (2) is difficult. However with the help of the second part of Eq. (2), it is possible to estimate the velocity of the shock wave front. For this purpose we can neglect the term containing plasma pressure for high laser intensity. Also, we assume that the laser field momentum flow is completely converted to ion momentum flow (by means of fast electrons), then from Eq. (2), we obtain the ion velocity behind the shock wave front,

$$\mu\approx(2\delta_T^{-2}\sqrt{1+A^2})^{0.5}. \tag{3}$$

For example, for laser intensity $I_L=5\times10^{18}$ W/cm^2 the ion velocity is $v_i\approx0.03c$. We should emphasize that expression (3) approximates ion velocity near a position of critical electron density $n_e=n_{\mathrm{cr}}$, where the ponderomotive pressure is applied. If we want to estimate the velocity inside overdense plasma, the law of conservation of momentum produces a factor $n_{\mathrm{cr}}/\mathrm{Z}n_i$ inside parenthesis in Eq. (3) (see also Ref. [9]).

An approximate analytical solution (2) is possible for laser fields of small intensities ($A<1$). In this case, the shock wave is feeble and the perturbation theory can be applied for solving Eq. (2). We substitute $\eta=\eta_p+\delta\eta$ and expand Eq. (2) into a series in $\delta\eta$, where η_p does not depend on A. For the first-order perturbation theory, we obtain the sound equation for $\delta\eta$. For the second order the density perturbation $\delta\eta$ is described by KdW equation in Ref. [10],

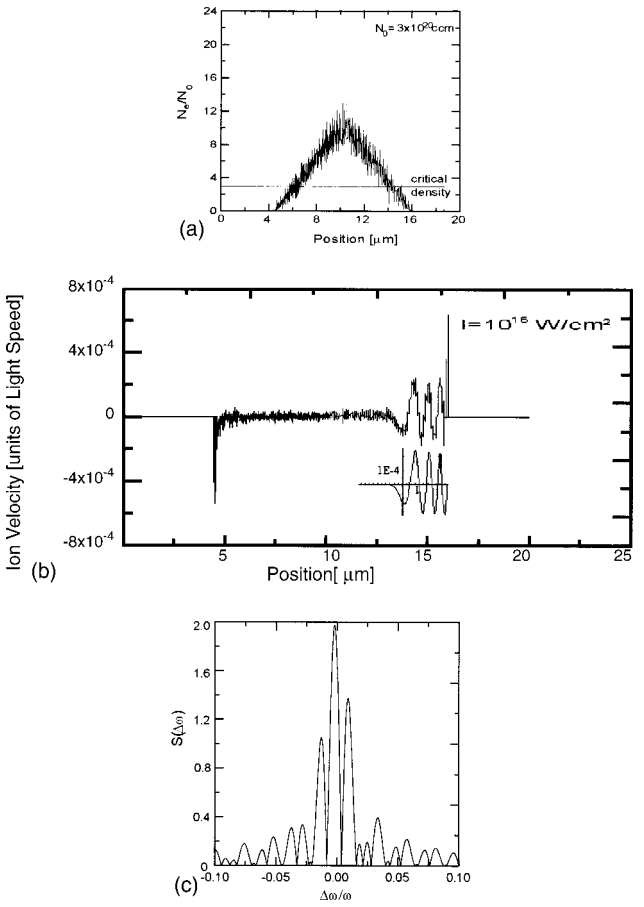

FIG. 1. Spatial distribution of ion density (a) and velocity (b), in plasma after 200 fs irradiation by the laser pulse with $I=10^{16}$ W/cm^2, $\lambda_0=1\,\mu$m with initial density scale length $L/\lambda_0=6$ in the vicinity of the critical density; (c) the time-integrated spectral intensity of backward scattered laser light

$$-\frac{\partial\delta\eta}{\partial\tau}+\frac{\partial\delta\eta}{\partial\xi}+\delta\eta\frac{\partial\delta\eta}{\partial\xi}+\beta\frac{\partial^3\delta\eta}{\partial\xi^3}+\frac{\alpha}{\pi}P\int_{-\infty}^{+\infty}\frac{\partial\delta\eta}{\partial\xi'}\frac{d\xi'}{(\xi-\xi')}=\frac{1}{4\delta_T^2}\frac{\partial A^2}{\partial\xi}, \tag{4}$$

where

$$\beta=0.5\delta_T^2\Omega_p,\alpha=\sqrt{\frac{\pi m}{8M}}Q_p.$$

Here we consider only the sound wave that propagates inside a dense plasma not outside (see Fig. 1). For Al plasma and actual experimental data we substitute $\omega_p/\omega_0=10$, $v_{\mathrm{Te}}/c=0.1$, then $\beta=0.05$ and $\alpha=0.03$. The term that contains an integral describes damping of nonlinear ion-sound oscillations and the term containing parameter β describes dispersion of ion sound. In chosen units, equation for ion hydrodynamics velocity μ coincides with Eq. (4).

Equation (4) is valid for $\delta\eta<1$, therefore we can use the expansion in A in Eq. (1) also. Then we get the equation for A,

$$\left(\frac{\partial^2}{\partial\xi^2}+2i\frac{\delta_s}{\Omega_p}\frac{\partial}{\partial\tau}+\frac{1}{\Omega_p^2}-1\right)A=\left(\delta\eta-\frac{A^2}{2}+\frac{\partial^2}{\partial\xi^2}\frac{A^2}{2}\right)A. \tag{5}$$

To determine the boundary conditions, we integrate Eq. (4) over ξ at the right-hand boundary of plasma

$$\delta\eta+\frac{(\delta\eta)^2}{2}+\beta\left.\frac{\partial^2\delta\eta}{\partial\xi^2}\right|_{\xi=0}=0.25\delta_T^{-2}A^2(\xi=0,\tau). \tag{6}$$

At the left boundary we set boundary conditions for the function and derivative to zero. The initial conditions also we put as $\delta\eta|_{t=0}=0$

The restriction on the laser wave amplitude in plasma, for which the perturbation of ion density in Eq. (2) remains weak, is as follows: $|A|\leqslant 2\delta_T$. This condition is valid for $I_L\leqslant 10^{17}$ W/cm^2 in plasma with steep density gradient.

The numerical solution of Eqs. (4) and (5) in such plasma has shown that, upon action of the laser pulse on plasma, there is a shock front followed by the oscillation of density. These oscillations transform into nonlinear structures (such as solitons) as laser intensity increases.

C. Analysis of moderate intensity laser pulse reflection from plasma

With density gradient decrease, one cannot neglect effects of preplasma with the acoustic waves generated. Accordingly, the right-hand side of Eq. (4) cannot be reduced to the boundary condition (6) now. An analytical estimation for such a case is possible via linearization of Eqs. (4) and (5) for low laser intensities $\leqslant 10^{16}$ W/cm^2. To analyze laser pulse reflection from such structures we consider first the model plasma density profile $\eta_p(\xi,\tau)$ created by the prepulse as

$$\eta_p(\xi,\tau)=\begin{cases}0, & \xi>\xi_p=\mu_p\tau+\xi_0\\ \xi_0\eta_{0p}/(\xi_p-\xi_c), & \xi_p>\xi>\xi_c\\ 1, & \xi<\xi_c=\mu_c\tau.\end{cases} \tag{7}$$

Here the reflected plasma surface moves with thermal velocity $\mu_{\rm cr}$ and the plasma boundary moves in the direction opposite to the laser wave at velocity μ_p. The preplasma has density η_{0p} and length ξ_0, where $(\mu_p-\mu_c)\tau_L<\xi_0$. Velocities, $1\geqslant\mu_p\gg\mu_c$, are determined by the laser prepulse. Pondermotive pressure cannot change the direction of μ_c here.

A linear analysis of sound and electromagnetic equations [5] shows that there are incident, $A_0(\xi,\tau)=A_0\sin(\chi(\xi-\nu_\alpha\tau))$, sound, $\delta\eta$, and scattered, A_1, interacting waves and the frequency of the sound and scattered waves can be determined from the usual conservation laws,

$$\omega_s=2\omega_{s0}\chi,$$
$$\omega_1=\omega_0\left\{1-[2(1-\mu_p)-\mu_c]\frac{\omega_{s0}}{\omega_0}\chi\right\}. \tag{8}$$

Here $\chi=\sqrt{1/\Omega_p^2-\eta_{0p}}$, $\omega_{s0}=c_s/l_s$, $l_s=c/\omega_{p0}$. From Eq. (8) we see that the spectral line of the reflected wave is shifted by the ion-sound frequency and if we take into account the preplasma length it is broadened as $c/\chi\ \xi_0$. The shifted line amplitude is about $A_0\delta\eta/\eta_p\ll 1$, where A_0 is the laser pulse amplitude. The higher sound harmonics are generated in the next orders of perturbation theory and the harmonic amplitude decreases with the order of the harmonics. According to Eq. (8), the sound wavelength equals half of laser wavelength. We should note that the linearized equation for sound waves can be easily solved. For plasma with linear density profile, which is used for numerical simulation, the vector potential has the following form: $A(\xi,\tau)\approx A_0{\rm Ai}[(\xi-\mu_c\tau)l^{-1/3}]$, where Ai$(x)$ is Airy function, $l=L/l_s$, L is the plasma density scale length.

A particular solution of the equation has the asymptotic form as following:

$$\begin{aligned}&\delta\eta\approx\eta_a A_0^2[(\xi-\mu_c\tau)l^{-1/3}]^{-1/2}\sin[4(\xi-\mu_c\tau)^{3/2}/3l^{1/2}],\\ &\qquad\xi\gg\mu_c\tau,\\ &\delta\eta\approx\eta_b A_0^2[(\xi-\mu_c\tau)l^{-1/3}]^{-1/2}\\ &\qquad\times\exp[-4(\xi-\mu_c\tau)^{3/2}/3l^{1/2}],\quad \xi\ll\mu_c\tau.\end{aligned} \tag{9}$$

At the right-hand side of the critical point, sound oscillations are harmonical with decreasing wavelength while at the left-hand side the oscillations exponentially decay.

To verify the analytical estimation, we perform the numerical simulation for the generation of sound waves in the plasma corona with the density profile given in Fig. 1(a) for the laser intensity 10^{16} W/cm^2.

As seen in Fig. 1(b), the wavelength of sound near at the plasma-vacuum boundary is ≈ 0.5 μm, a half of laser wavelength [see, Eqs. (8) and (9)]. In Fig. 1(b), one can observe an increase of the sound wavelength at the critical point and the wave decay at the left side of critical point, which agree well with the solution of Eq. (9) [see subframe of Fig. 1(b)].

We note that most peaks of velocity at the left and right sides in Fig. 1(b) correspond to ions leaving the plasma under the action of the bipolar field produced by hot electrons.

The spectrum of reflected light is given in Fig. 1(c). The sound speed is equal to $c_s\sim 3\ 10^{-4}c$ ($T_e\sim 200$ eV, Al target), thus $\omega_s/\omega_0\sim 2c_c/c\sim 6\times 10^{-4}$. Therefore, the redshift in the spectrum could be $\Delta\omega/\omega_0\approx 10^{-3}$ for the laser intensity 10^{16} W/cm^2 that agrees with the shift of the central peak in Fig. 1(c). Since this shift is rather small, the spectral effect originating from the short duration (here $t_L=200$ fs) of the laser pulse becomes important leading the modulation with typical period $\delta\omega_L\approx\pi/t_L$ and spectral line broadening. Thus for the laser intensities considered, the modulation and spectral width are dominated by finite pulse length rather than by the generation of acoustic wave, provoking relatively small red spectral shift.

The dispersion term of Eq. (4) is essential for high plasma temperature. As shown in Ref. [10], a solution of Eq. (4) in this case is expressed through Airy function

$$\delta\eta(\xi,\tau)=\delta\eta_0\mathrm{Ai}\left(\frac{\xi+(1-\mu_p)\tau}{(3\beta\tau)^{1/3}}\right), \tag{10}$$

where $\delta\eta_0\sim A_0^2$. Such density profile, containing downward peaks, is qualitatively similar to the picture of calculated wave distribution. For the analysis of the spectrum of scattered radiation we use the perturbation theory of Eqs. (4) and (5), taking $\delta\eta$ from Eq. (9) and A we take as standing wave: $A(\xi,\tau)=A_0\sin[\chi(\xi-\mu_c\tau)]$, then for the scattered wave vector potential, we obtain the next formula,

$$A_1(\xi,\tau)=-\int_{-\infty}^{\tau}d\tau'\int_{\nu_{\mathrm{or}}}^{\infty}d\xi' G(\xi,\xi';\tau,\tau')\times\delta\eta(\xi',\tau')A(\xi',\tau'),$$

where the Green function is

$$G(\xi,\xi';\tau,\tau')=\sqrt{\frac{\delta_s}{2\pi i\Omega_p(\tau-\tau')}}\left(\exp\frac{i\Omega_p(\tau-\tau')\chi^2}{2\delta_s}\right)\times\left(\exp\frac{i\delta_s(\xi-\mu_c\tau-\xi'+\mu_c\tau')^2}{2\Omega_p(\tau-\tau')}-\exp\frac{i\delta_s(\xi+\xi'-\mu_c\tau-\mu_c\tau')^2}{2\Omega_p(\tau-\tau')}\right).$$

We do Fourier transformation of A_1 to detect the spectrum of reflected radiation. As a result, the Fourier component of the vector potential of scattered radiation for large ξ becomes

$$\hat{A}(\xi,\Omega)\approx\hat{A}_0\delta\eta_0\exp(i\chi\xi)\beta^{-1/3}\times[3\beta\chi^3+\chi\{2(1-\mu_p)+\mu_c\}-\Omega]^{-4/3}.$$

Here $\Omega=\Delta\omega/\omega_{s0}=(\omega_1-\omega_0)/\omega_{s0}$. The maximum of the spectrum $\omega_{1\,\max}$ is shifted to the ''red'' side from laser frequency by a distance $\Delta\omega$, broadened, and its amplitude decreases with $\sim\omega_1^{-4/3}$. For the shift we have the following expression:

$$\Delta\omega\approx-\omega_{s0}[3\beta\chi^3+\chi\{2(1-\mu_p)+\mu_c\}]. \tag{11}$$

Here $\Delta\omega/\omega_0\sim c_s/c\sim10^{-3}$. Near to the spectrum peak our description is inapplicable, but the wings of the spectrum are described correctly. By comparing Eqs. (8) and (11) we see that sound dispersion gives an additional shift of the reflected spectrum.

Now we consider some nonlinear solutions of Eqs. (4) and (5), which can be obtained for higher laser intensity. The range of laser intensities, where nonlinearity becomes important but still is small, is $I=410^{16}$ W/cm^2 for the plasma with a smooth boundary and $I=10^{17}$ W/cm^2 for the plasma with a steep density gradient.

Analytical solutions of Eq. (4) are derivable for plasmas with steep density gradient, with the skin length being smaller than the free path of an acoustic wave. In this case, the right-hand side of Eq. (4) can be substituted by the boundary condition (6). Then we can apply the fact that the nonlinear and dispersion terms in Eq. (4) are small and substitute the derivative $\partial/\partial\xi$ by $\partial/\partial\tau$. Neglecting by decay, Eq. (4) transforms to the standard KdV equation with the boundary condition given by Eq. (6) without nonlinearity. This equation can be already solved by the ''inverse scattering'' method [10]. Qualitatively such a solution is a sound wave with increasing wavelength and amplitude, which breaks into narrow and tall solitons appearing with a decreasing amplitude. The amplitudes and velocities of these solitons are determined by the discrete spectrum of an effective potential.

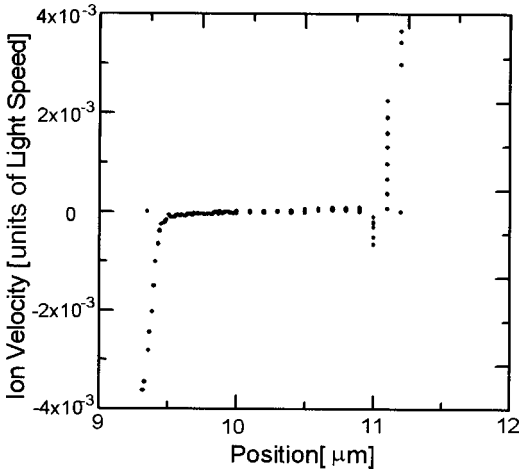

FIG. 2. Spatial distribution of ion velocity in plasma after 200 fs irradiation by the laser pulse with $I=10^{17}$ W/cm^2, $\lambda_0=1$ μm with initial density scale length $L/\lambda_0=0.5$ in the vicinity of the critical density.

For short laser pulses ($t_L<500$ fs) when characteristic ion time much exceeds the pulse duration, the soliton solution can be derived in an analytical form via applying δ-function approximation for the laser pulse shape,

$$\delta\eta|_{\xi=0}=\frac{mc^2}{4T_c}\langle A^2(\xi=0)\rangle\delta(\tau/\tau_i). \tag{12}$$

A discrete spectrum of the Schrödinger equation for the effective potential (profile) (12) consists of only one value, $\kappa=mc^2\tau_i/24\beta T_e\langle A^2(\xi=0)\rangle$ and the corresponding soliton solution is as follows:

$$\delta\eta(\xi,\tau)=-\kappa\,\mathrm{ch}^{-2}\{\sqrt{\kappa/12}[\xi+\tau(1+\kappa/3)+\xi_0]\}. \tag{13}$$

A similar structure obtained in the simulation is shown in Fig. 2.

For the analysis of the spectrum of scattered radiation we use the perturbation theory equation (5) in the case of sharp gradient, where $\delta\eta$ has been from Eq. (13) and $\eta_{\mathrm{op}}=1$, $A_0(\xi,\tau)\approx(A_{0,in}/\Omega_p)\exp(\xi-\mu_c\tau)$.

For the solution through the Green function we have the following expression:

$$A_1(\xi,\tau)=-\int_{-\infty}^{t}d\tau'\int_{-\infty}^{\nu_\alpha t}d\xi' G(\xi,\xi';\tau,\tau')\times\delta\eta(\xi',\tau')A_0(\xi',\tau'). \tag{14}$$

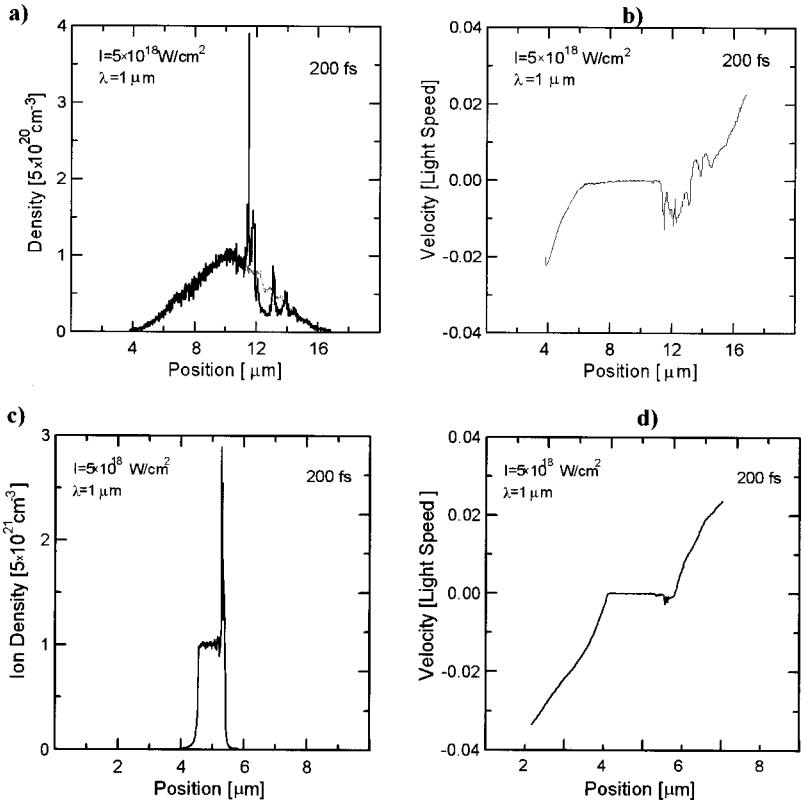

FIG. 3. Spatial distribution of ion density (a), (c) and velocity (b), (d) in plasma after 200 fs irradiation by the laser pulse with $I=5\times10^{18}$ W/cm^2, $\lambda_0=1\ \mu$m with different initial density scale length $L=[d\ln(N)/dz]^{-1}$ in the vicinity of the critical density.

We do Fourier transformation of Eq. (14) to detect the spectrum of reflected radiation. As a result the Fourier component of the vector potential of scattered radiation for large ξ becomes

$$\hat{A}_1(\xi,\Omega)\approx\frac{A_{0,\mathrm{n}}}{\Omega_p}\exp(i\chi\xi)\times\frac{6\pi(\Omega-\chi\mu_c)}{\kappa sh[\pi(\Omega-\chi\mu_c)/2\sqrt{\kappa/12}(1+\kappa/3)]}.$$

Thus, these estimations show that even a relatively low nonlinearity of sound waves with an increase of laser intensity provokes broadening in the spectrum of reflected light, which is $\sim\omega_p\delta_g\kappa^{1/2}$.

D. Analysis of high intensity laser pulse reflection from overdense plasma cavity

The theory of spectrum of the backward reflected signal presented above is applicable to plasmas irradiated by a laser pulse with intensity below 10^{17} W/cm^2 because it uses the perturbation series to solve the set of hydrodynamic equations. However, for higher laser pulse intensity, over 10^{18} W/cm^2, which is more interesting at present, hydrodynamic equations cannot be reduced to the KdW equation. We cannot get a rigorous analytical solution of Eq. (4) either. Instead, we perform numerical simulation of the reflection process with the described 1D PIC code. To explain results obtained from the calculation, we are using the hydrodynamic equations again for the estimation of the order of magnitude of the plasma parameters and for their comparison with the numerical ones. For that, we use the plasma density profile $\eta_p(\xi,\tau)$ in the form close to Eq. (7),

$$\eta_p(\xi,\tau)=\begin{cases}0, & \xi>\xi_p\\ \eta_c-(\eta_c-\eta_{p0})\dfrac{\xi-\xi_c}{\xi_p-\xi_c}, & \xi_p>\xi>\xi_c\\ 1-(1-\eta_c)\dfrac{\xi-\xi_a}{\xi_c-\xi_a}, & \xi_c>\xi>\xi_a\\ 1, & \xi<\xi_a,\end{cases}\tag{15}$$

where $\xi_p(\tau)$ is the position where the plasma density starts growing from the value η_{0p}, $\xi_c(\tau)$ is the position in the vicinity of the critical density, $\xi_a(\tau)$ is the position of the ablation front, $\eta_c=n_{\mathrm{cr}}/\mathrm{Z}n_{i0}$. Such a form of the density profile agrees qualitatively with the result of numerical simulation given in Fig. 3(a).

One can see in the figures that the change in the density profile $\delta\eta/\eta$ at high laser intensity is about a factor of 2–3, the case for a strong shock wave. The shock wave velocity exceeds the sound velocity by one order of magnitude. The character of shock wave motion also distinguishes it from that for the case of weaker laser fields. In the vicinity of critical density due to ponderomotive force, the density profile becomes steeper and this density cliff moves into the plasma bulk (during the main part of the laser pulse) with approximately constant speed (see figures). Plasma expansion into vacuum runs supersonically at acceleration $g\sim10^{21}$ cm/s^2. The source of this acceleration is the strong bipolar field produced by energetic electrons leaving the

plasma. This field drives ions towards the plasma boundary. At the sharp boundary, the magnitude of this field is maximal and, hence, the expansion velocity is the largest. One can see this by comparing the velocity at the smooth and sharp boundaries given in Figs. 3(a) and 3(c).

It is also apparent that the velocity in the vicinity of the critical density in a plasma with sharp boundary is much smaller ($\sim$5 times) than that in a plasma with smooth boundary, as seen in Fig. 3. This fact is essential for understanding the behavior of the reflected laser light. Besides, the perturbation of plasma density in the bulk in longer time (500 fs) transforms to a set of solitary waves with descending amplitudes. This agrees qualitatively with the theory of the KdW equation. Following the results of the calculation as given in Fig. 3, we choose an approximation for the coordinates $\xi_p(\tau)$ and $\xi_c(\tau)$ defined in Eq. (15) in the following form:

$$\xi_p(\tau)=\mu_p\tau+\frac{g\tau^2}{2},$$

$$\xi_c(\tau)=-\mu_c\tau, \tag{16}$$

where g, μ_p are the acceleration and velocity of expanding plasma, μ_c is the velocity in the vicinity of the critical density. These parameters can be estimated directly from the hydrodynamics equation, from the ion and electron momentum flow conservation given by Eq. (3). Then in chosen units of time and coordinate, we get

$$\mu_p=\left(\frac{2Zm_ec^2n_h}{\tilde{A}m_pc_s^2n_{\rm cr}}\sqrt{1+A_0^2}\right)^{0.5},$$

$$\mu_c=\left(\frac{2Zm_ec^2n_{\rm cr}}{\tilde{A}m_pc_s^2n_i}\sqrt{1+A_0^2}\right)^{0.5}, \tag{17}$$

$$g=\frac{Zm_ec^3}{\tilde{A}m_pc_s^2l_s\omega_p}\sqrt{1+A_0^2},$$

where n_h is the density of hot electrons emitted to vacuum. We should note that the acceleration in the vicinity of critical density exists, especially at the beginning of the process. However, this acceleration is much less than that of the layer at the plasma surface. In Eq. (16), we keep the largest acceleration only.

Estimation Eq. (17) of ion velocity is confirmed by our PIC simulations. One can see in Fig. 3 that numerical simulation gives the magnitude of the shock front velocity as $v_c \approx 0.014c$ (time 200 fs). The estimation based on Eqs. (17) agrees well with these numerical results at $n_{\rm cr}\sim Zn_i$.

For a sharp boundary (steep density gradient), the quantity $n_{\rm cr}/Zn_i \ll 1$ and the velocity μ_c, according to Eq. (17), decreases. The acceleration of the plasma boundary follows Eq. (17) as well, though we have to accept that this acceleration is not constant during the laser pulse and changes notably. Thus, the estimation of the spectrum width and shift can be obtained only as an order of magnitude.

For estimation of the reflected light spectrum, we apply the following simple model. The laser wave is reflected partially already from the underdense plasma layer (according to the Fresnel formula, its reflectivity is proportional to plasma density in the layer), then a certain portion of the radiation is absorbed, while most of the radiation is reflected in the vicinity of critical density. The motion of the underdense layer with velocity μ_p leads to a blue Doppler shift of reflected light $\Delta\omega_b=\omega_1-\omega_0$ (FS),

$$\frac{\Delta\omega_b}{\omega_0}=\delta_s\mu_p. \tag{18}$$

In contrast, the motion in the vicinity of critical density leads to a red Doppler shift $\Delta\omega_r=\omega_1-\omega_0$(FS):

$$\frac{\Delta\omega_r}{\omega_0}=-\delta_s\mu_c\sqrt{1-\eta_p\Omega_p^2}. \tag{19}$$

The ratio of amplitudes of the red and blue parts of the spectrum is apparently determined by the ratio of corresponding coefficients of refraction, from the underdense layer and from the critical surface. The broadening of the backward reflected laser light is driven by the acceleration of the reflecting surface as a whole. The model shows the spectral width to be proportional to the square root of the product of the wave vector and acceleration. Hence, the linewidth $\delta\omega$ [full width at half maximum (FWHM)] is given by following equation:

$$\frac{\delta\omega}{\omega_0}=(\sqrt{1-\eta_p\Omega_p^2}\Omega_p g)^{1/2}. \tag{20}$$

The full spectrum of the backward reflected laser light is given in Fig. 4 for various laser intensities and plasma density gradients. The spectrum changes with plasma and laser parameters depending on the change in the character of the plasma motion. Since an increase in the laser intensity gives an increase in the plasma velocity and acceleration [see Eqs. (18)–(20)], the shift and width increase consequently as seen in Fig. 4. An increase in the density gradient (a decrease in the density gradient scale length) leads to a decrease in the velocity of the critical surface and to an increase of plasma expansion velocity. As a result, the redshift decreases and the spectrum moves to the blue side. Plasma density in the underdense layer in plasma with a sharp boundary is larger than that of plasma with a smooth boundary; the weight of blue-shifted radiation in this plasma goes up as seen in Fig. 4. According to results presented in Fig. 4, we can identify plasmas with steep density gradient (density gradient scale length L less than laser wavelength λ_0). For such plasmas, there is no red-shifted maximum in the backward scattered laser light in the range of its intensity 10^{18}–10^{19} W/cm^2. The dependence of the shift (FS) and width (FWHM) of scattered laser light on the laser intensity and density gradient are shown in Figs. 5 and 6. These results agree fairly well with analytical formulas of Eqs. (17), (19), and (20). First, we check the dependence on the laser intensity. According to Eqs. (17), (19), and (20) with $n_{\rm cr}\sim\sqrt{1+A^2}$, one can derive

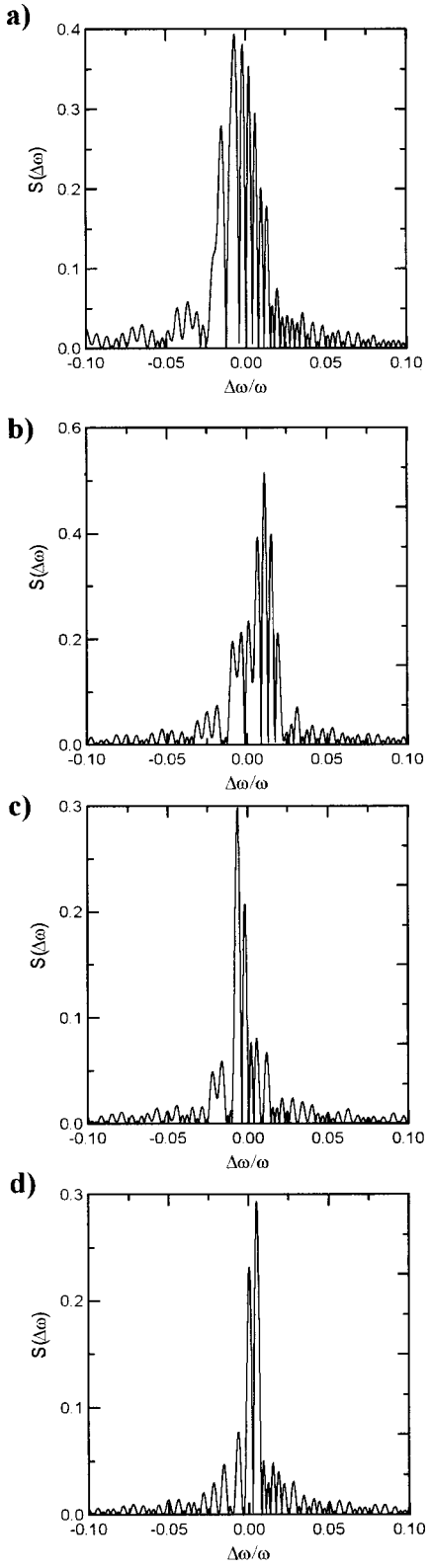

FIG. 4. The time-integrated spectral intensity of backward scattered laser light after $t=400$ fs: $I=10^{19}$ W/cm^2, $L/\lambda_0=3$ (a); $L/\lambda_0=1$ (b); $I=2\times10^{18}$ W/cm^2, $L/\lambda_0=3$ (c); $L/\lambda_0=1$ (d).

this dependence for the shift (FS) $\Delta\omega_r/\omega_0\sim A\sim\sqrt{I}$, and for the width (FWHM), $\delta\omega/\omega_0\sim A^{1/2}\sim I^{1/4}$.

As seen in Figs. 5 and 6, the shift FWHM is upwards

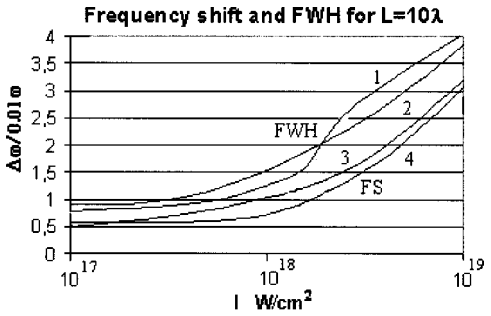

FIG. 5. Dependence of time-integrated spectral width (FWHM) and shift (FS) on the pulse intensity at $L/\lambda_0=3$ after $t=400$ fs. Simulation curves 1,3; analytical curves 2,4.

convex indeed. The agreement of calculated and simulated quantities is good as well. At the velocities $v_c\sim0.014c$, $v_p\sim0.03c$, the shift from Eq. (19) is about 0.02 of the laser frequency that is very near to the calculated value. The analytically derived width is larger than the shift in the factor $(4\omega_p/3\omega_0)^{1/2}$ that also agrees well with the simulation results. Since the plasma is overdense, the FWHM curve is above the FS curve. The dependence of the shift and width on the density gradient presented in Fig. 6 also is in accordance with the estimation of Eqs. (17), (19), and (20). The steeper that density gradient is, the weaker the laser field penetrating the plasma [value $n_{\rm cr}/Zn_i$ in Eq. (17) is smaller for stepper gradients]. Consequently, the velocity of the critical surface and, hence, the shift of spectrum to red wing becomes less. The broadening corresponding to the acceleration of underdense layer depends on the laser intensity being weaker than that of small density gradients because a decrease in the laser field at the plasma surface is compensated partially by a growth in the bipolar field, which accelerates ions.

Thus, via experimentally measured shift and width of spectrum of the backward scattered laser light, one can estimate the velocity and acceleration of a plasma and also the scale length of plasma inhomogeneity and the effect of the laser prepulse.

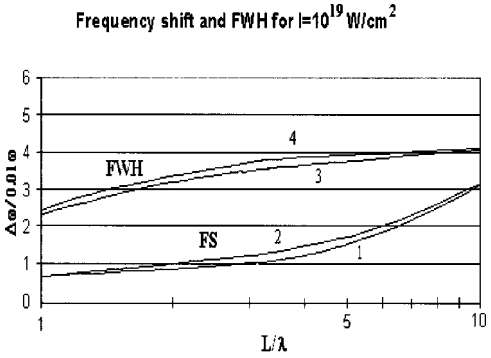

FIG. 6. Dependence of time-integrated spectral width (FWHM) and shift (FS) on the pulse intensity on the density gradient in the vicinity of critical density, $L=[d\ln(N)/dz]^{-1}$ at $N_e=N_{\rm cr}$, after $t=400$ fs, $I=10^{19}$ W/cm^2. Simulation curves 1,3; analytical curves 2,4.

CONCLUSIONS

This theoretical analysis of short high power laser pulse reflection from overdense plasmas resulted in the following conclusions.

(1) Ponderomotive pressure of laser light near critical density produces a shock wave that propagates deeply into plasma. This process changes the profile of plasma density and creates two areas: transparent underdense plasma and above-critical dense plasma. The critical density surface separating these areas moves with supersonic speed deeply into the plasma along with the front of the shock wave at ultrahigh laser intensity. In undercritical and above-critical areas intense nonlinear plasma density waves are generated. In the transparent area the degree of nonlinearity is higher, due to higher field amplitude.

(2) The indicated processes affect the spectrum of scattered radiation in the following way:

(i) At low laser intensity, they are ambipolar plasma expansion and ion sound harmonic generation in underdense plasma. In this case there is a small redshift of the maximum in the scattered light spectrum.

(ii) At high laser intensity, the critical surface movement produces red Doppler frequency shift of scattered light, and the plasma expansion produces a blueshift. The result of the interference of these two processes depends on the plasma density gradient: these shifts may compensate each other in steep density gradient ($L<\lambda_0$) plasmas while in long density gradient plasmas ($L>\lambda_0$) the redshift is dominant.

(iii) At low laser intensity, nonlinear ion sound in an underdense plasma produces harmonics in the spectrum of the scattered radiation that dominate spectrum width. Ion-sound dispersion at high plasma temperature produces a small redshift also. At high laser intensity, the spectrum width is determined by the acceleration of the underdense plasma layer.

(3) Low frequency modulation of scattered light spectrum and additional spectral width is produced by finite duration of a laser pulse.

(4) The measurements of the spectrum shift of reflected radiation thus allow us to determine the speed and acceleration of critical surface and underdense layer, and therefore to determine the plasma gradient.

(5) The absence of the redshift in the maximum of the spectrum for $I>10^{18}$ W/cm^{-2} displays the steep density gradient in plasmas and the negligible effect of the laser prepulse. This fact may be useful in the diagnostics of pulse contrast ratio of intense lasers.

ACKNOWLEDGMENTS

The authors acknowledge useful discussion with Dr. A. Sasaki and Professor L. Roso.

[1] M. P. Kalashnikov *et al.*, Phys. Rev. Lett. **73**, 260 (1994).
[2] R. Lichters, J. Meyer-ter-Vehn, A. Puchov, Phys. Plasmas **3**, 3425 (1996).
[3] A. A. Andreev *et al.*, *Superstrong Field in Plasma*, edited by M. Lontano *et al.*, AIP Conf. Proc. No. 426 (AIP, Woodbury, NY, 1998), p. 61.
[4] K. Tanaka *et al.*, Phys. Plasmas **7**, 2014 (2000).
[5] A. A. Andreev and A. N. Sutyagin, Quantum Electron. **24**, 155 (1997).
[6] A. A. Andreev *et al.*, Plasma Phys. Controlled Fusion **44**, 330 (2002).
[7] R. J. Kingham *et al.*, Phys. Rev. Lett. **86**, 810 (2001).
[8] Ya. B. Zeldovich and Yu. P. Raiser, *Physics of Shock Waves and High-Temperature Hydrodynamic Phenomena* (Academic Press, New York, 1966), Vols. 1 and 2.
[9] S. C. Wilks and W. L. Kruer, Phys. Rev. Lett. **69**, 1383 (1992).
[10] S. P. Novikov *et al.*, *Theory of Solitons: The Inverse Scattering Methods* (Consultants Bureau, New York, 1984).
[11] A. Zhidkov *et al.*, Phys. Rev. E **61**, R2224 (2000).